Photon- and electron-stimulated desorption from laboratory models of interstellar ice grains

J. D. Thrower,[a] A. G. M. Abdulgalil, M. P. Collings, and M. R. S. McCoustra[b]
School of Engineering and Physical Sciences, Heriot-Watt University, Riccarton, Edinburgh EH 14 4AS, United Kingdom

D. J. Burke[c] and W. A. Brown
Department of Chemistry, University College London, 20 Gordon Street, London W1CH 0AJ, United Kingdom

A. Dawes, P. J. Holtom, P. Kendall, and N. J. Mason
Department of Physics and Astronomy, The Open University, Walton Hall, Milton Keynes MK7 6AA, United Kingdom

F. Jamme
SOLEIL Synchrotron, BP 48, L'Orme des Merisiers, F-91192 Gif surf Yvette Cédex, France

H. J. Fraser
Department of Physics, Scottish Universities Physics Alliance (SUPA), University of Strathclyde, John Anderson Building, 107 Rottenrow East, Glasgow G4 0NG, United Kingdom

F. J. M. Rutten
School of Pharmacy and iEPSAM, Keele University, Keele ST5 5BG, United Kingdom

(Received 15 October 2009; accepted 1 February 2010; published 29 June 2010)

The nonthermal desorption of water from ice films induced by photon and low energy electron irradiation has been studied under conditions mimicking those found in dense interstellar clouds. Water desorption following photon irradiation at 250 nm relies on the presence of an absorbing species within the H_2O ice, in this case benzene. Desorption cross sections are obtained and used to derive first order rate coefficients for the desorption processes. Kinetic modeling has been used to compare the efficiencies of these desorption mechanisms with others known to be in operation in dense clouds. © *2010 American Vacuum Society.* [DOI: 10.1116/1.3336466]

I. INTRODUCTION

Since most astrophysical environments evolve on a time scale that is far too slow to allow observation of changes, their dynamics are studied with the use of modeling. Such models are dependent on the incorporation of reliable experimental data. In this article, we report on the results of a series of experiments using ultrahigh vacuum (UHV) surface science techniques to investigate nonthermal desorption mechanisms of relevance to interstellar grains in molecular clouds within the interstellar medium (ISM). Processes occurring on the surfaces of such grains are now widely viewed as playing a crucial role in the surprisingly rich chemistry of these environments, where, ultimately, gravitational collapse leads to star formation.[1] For example, the synthesis of the most abundant interstellar molecule, H_2, for which there are no efficient gas phase routes, has been thought for many years to be efficient on the surfaces of such grains.[2,3] Infrared observations have revealed icy mantles composed primarily of H_2O ice, along with a range of other simple species, which form around a carbonaceous material or silicate mineral grain core.[4] The past two decades have seen extensive experimental and theoretical efforts aimed at understanding the nature of these mantles and the mechanisms for the formation of the range of species found both within interstellar ices and in the gas phase of dense interstellar regions. While the heterogeneous and poorly understood nature of such surfaces is experimentally inconvenient, and the application of results still requires many assumptions and simplifications; the experimental data, such as those that can be provided by a surface science laboratory, remain immensely significant in astrophysics.

Desorption from grain mantles provides the necessary mechanism by which species formed in the condensed phase can reach the gas phase. Thermal desorption, which occurs gradually as a result of gravitational heating during cloud collapse, has been studied experimentally through temperature programed desorption experiments.[5–9] The kinetic parameters derived from such experiments can be applied in astrochemical models with astrophysically relevant heating rates of 0.1–1 K/century. In cold regions, however, thermal desorption cannot account for the gas phase abundance of many species including H_2O.[10,11] Given the lack of efficient gas phase formation routes for H_2O, nonthermal desorption mechanisms are frequently invoked to provide the necessary desorption efficiency.

[a]Present address: Department of Physics and Astronomy, Aarhus University, 8000 Aarhus C, Denmark.
[b]Author to whom correspondence should be addressed; electronic mail: m.r.s.mccoustra@hw.ac.uk
[c]Present address: Laboratory for Atomic and Surface Physics, University of Virginia, Thornton Hall B113, Charlottesville, VA 22904-4238.

Photon-stimulated desorption (PSD) under astrophysically relevant conditions has received little attention until recently. The photon absorption cross section for H_2O ice is negligible for wavelengths longer than 170 nm.[12] As a result, the experiments performed have utilized relatively short UV wavelengths centered around that of Lyman-α radiation and have demonstrated the desorption of H_2O molecules.[13–16] The mechanisms for desorption at these wavelengths have been discussed at length, with time-of-flight (ToF) measurements indicating the desorption of intact H_2O molecules and photoproducts with significant translational energies.[17–19] Lyman-α radiation, which results from the recombination of electrons and protons produced by cosmic ray ionization, is thought to dominate photon-stimulated processes deep within molecular clouds where the interstellar radiation field (ISRF) is strongly attenuated.[20] Attenuation is generally reported in terms of the extinction coefficient A_v, which reflects the reduction in photon flux in the visible region as a result of absorption and scattering. UV photons with energies close to Lyman-α are also generated during the fluorescence of H_2 molecules excited through collisions with cosmic ray particles.[21] At the edges of clouds, and within more diffuse regions, the ISRF is likely to have an important impact on the observed desorption rate.[22] In the experiments described here, we use photons with a wavelength of around 250 nm to represent the interstellar radiation field. We have shown previously that the presence of C_6H_6 can lead to significant H_2O desorption at these longer wavelengths.[23,24] In this article, we aim to quantify the efficiency of this process by obtaining the relevant H_2O desorption cross section.

The low energy electron irradiation of H_2O ice films has also been studied extensively. Experiments have generally focused on the desorption of ionic and neutral dissociation products including H^-,[25] H, and O.[26] The formation of H_2 (Ref. 27) and O_2,[28] enhanced by trapping within a porous ice matrix,[29] has also been observed. Intact H_2O molecules[30] and protonated H_2O clusters[31] are also known to desorb during electron irradiation. These studies have focused on the nature of the products formed during irradiation, the dynamics of desorbing species, and the electron energy dependence of product yields in the threshold region. Here we report cross sections for the desorption of H_2O as a result of the low energy electron irradiation of pure amorphous solid water (ASW). We demonstrate that electron-stimulated processes are likely to play an important role in the desorption of H_2O ice deep within dense clouds, where low energy secondary electrons exist as a result of ionization during the passage of cosmic rays through the ice. The results presented here suggest that this process may be at least as, if not more, important than that induced by Lyman-α photons.

The icy mantle around interstellar grains is represented very simply in these experiments. C_6H_6 has been used as a model for complex molecules within ice mantles, particularly polycyclic aromatic hydrocarbons (PAHs), which are now widely accepted as being present in many astrophysical environments[32] and account for up to 20% of the carbon in the galaxy.[33,34] C_6H_6, rather than larger PAHs, was used here primarily for the experimental convenience that results from its relatively high vapor pressure. Nonthermal desorption kinetics for H_2O following irradiation with low energy electrons in the range of 100–300 eV and as a result of photon absorption by C_6H_6 are presented. Simple kinetic models are developed, with reference to previous studies existing in literature, to highlight the relative efficiencies of the different desorption mechanisms probed in this and previous studies.

II. EXPERIMENT

The experiments described in this article were conducted in two UHV chambers. A base pressure of 1×10^{-10} mbar was readily achievable in both systems. Photon-irradiation experiments were performed in an UHV system, which has been described previously,[24] in the Central Laser Facility (CLF) at the Rutherford Appleton Laboratories (RAL). The experimental procedures were as described for our previously reported ToF measurements. Briefly, multilayer films of C_6H_6 and H_2O were deposited on a sapphire substrate maintained at a temperature of ~80 K by backfilling the chamber to a pressure of 4×10^{-7} mbar for 500 s. Literature values for the densities of C_6H_6 (Ref. 35) and compact amorphous solid water (cASW) (Ref. 36) indicate film thicknesses for the two species of 7 and 21 nm, respectively, assuming a sticking probability of unity. Layered systems of benzene (B) and water (W) on the sapphire substrate (denoted by S) were used throughout the experiments and are denoted as follows: water alone (S/W); sequential adsorption of benzene, followed by water (S/B/W); and sequential adsorption of water then benzene (S/W/B). The PSD signals reported in the current study and the previously reported ToF profiles were recorded simultaneously.

Films were irradiated with the frequency-doubled output of a Nd^{3+}:YAG (YAG denotes yttrium aluminum garnet) pumped dye laser. A repetition rate of 10 Hz was used throughout. The UV beam obtained was incident at 45° to the surface normal and focused to a spot having an area of ~0.5 mm^2. Pulse energies of 1.1 and 1.8 mJ, corresponding to irradiances of 360 and 220 mJ cm^{-2} $pulse^{-1}$, were used, with a typical pulse-to-pulse variation of ±10%. Three irradiation wavelengths were employed in these experiments. 250.0 nm was used as the "on-resonance" wavelength, tuned to one of the components of the $B_{2u}\leftarrow A_{1g}$ band of C_6H_6, which is a vibronically allowed $\pi\rightarrow\pi^*$ transition. 248.8 nm was used as a "near-resonance" wavelength, being situated at a local minimum in the absorption cross section of C_6H_6, while 275.0 nm was used as an "off-resonance" reference wavelength. These wavelengths were selected with reference to the recently obtained vacuum ultraviolet absorption spectra of condensed C_6H_6.[37] It was not possible to use the higher pulse energy at 275.0 nm as a result of the accumulation of optical damage to the beam steering mirrors.

Photon-stimulated desorption traces were obtained with a quadrupole mass spectrometer (QMS) positioned in direct line-of-sight of the sapphire substrate. The line-of-sight was defined by a liquid nitrogen cooled Cu tube, designed to constrain detection to molecules desorbing from the substrate

of interest. Data were acquired for, typically, 20 s of irradiation by which time the desorption rate had dropped below the detection limit. The data were averaged over 30 laser spots, forming a grid across the substrate, to increase the signal quality.

Low-energy electron irradiation experiments were performed using a second UHV system at Heriot-Watt University.[38,39] The substrate was an amorphous SiO_2 film with a thickness of ~200 nm deposited onto a polished stainless steel disk by electron beam evaporation. We have developed this substrate, which has been characterized elsewhere,[39] as a simple interstellar grain mimic representing the silicate grain population. While this substrate is different to that used in the photon-irradiation experiments, the ice film thicknesses used in these experiments are sufficiently thick that substrate effects can be considered to be negligible. Therefore, in both the PSD and electron-stimulated desorption (ESD) experiments presented here, it is the bulk ice processes that are examined. The substrate reached a base temperature of ~115 K using a liquid nitrogen cryostat. cASW films were deposited using an effusive molecular beam with a flux of $(3.4 \pm 1) \times 10^{17}$ molecules m^{-2} s^{-1} and spatial dimensions sufficient to fill the surface area of the substrate. Beam exposures of 2000 s were used, corresponding to a cASW film thickness of ~16 nm, comparable to that used in the photon-irradiation experiments. C_6H_6 films were deposited using the backfilling procedure described above, with exposures reported in Langmuir units (1 L $= 10^{-6}$ torr s). In all cases, the C_6H_6 films were grown on top of a predeposited cASW film.

The deposited films were irradiated with a low energy electron beam produced using a dedicated electron gun (Kimball Physics, Inc.; ELG-2) mounted such that the beam was incident at around 45° to the surface normal. Electron energies of between 200 and 350 eV, with an energy spread of 0.5 eV, were obtained with the sample grounded through a picoammeter for beam current measurements. No significant differences in the beam current were observed between measurements made during the irradiation of the SiO_2 surface and the uncoated rear surface of the disc. Continuous beam irradiation with a beam current in the range of 100–200 nA, corresponding to electron fluxes of $(0.6-1.2) \times 10^{14}$ electrons cm^{-2} s^{-1}, was used throughout, with no evidence for effects that could be attributed to charging.

The desorption of C_6H_6 and H_2O was monitored using reflection-absorption infrared spectroscopy (RAIRS) measurements. RAIR spectra were obtained with a Fourier-transform infrared spectrometer interfaced to an external mercury cadmium telluride detector, with the IR beam being reflected of the surface at an angle of ~84° to the surface normal. Spectra were acquired with a resolution of 2 cm^{-1} and the coaddition of 1024 scans. The same initial film could be used for a complete experiment by obtaining a sample spectrum prior to irradiation and after successive periods of irradiation.

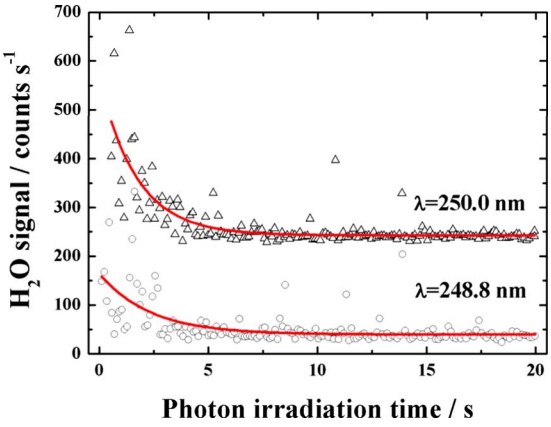

FIG. 1. (Color online) Photon-stimulated desorption traces for H_2O desorbed as a result of the indirect-adsorbate-mediated desorption channel involving C_6H_6. Traces obtained with irradiation wavelengths of 250.0 nm (open triangles) and 248.8 nm (open circles) are displayed. The solid lines are the fitted exponential decay functions. Both traces have been offset for clarity.

On both systems, the analytical grade C_6H_6 (Fluka) and de-ionized H_2O used in the experiments were purified by multiple freeze-thaw cycles under vacuum to remove dissolved contaminants.

III. RESULTS

A. Photon-stimulated desorption

Figure 1 shows H_2O PSD traces for the S/B/W system obtained with irradiation wavelengths of 250.0 and 248.8 nm and a pulse energy of 1.8 mJ. Similar traces were obtained, with a significantly smaller signal-to-noise ratio for a pulse energy of 1.1 mJ. No H_2O desorption was observed for an irradiation wavelength of 275.0 nm and a pulse energy of 1.1 mJ, where the absorption cross sections of both C_6H_6 and H_2O are negligible. Similarly, no significant H_2O desorption was observed when no C_6H_6 was present, confirming the presence of an indirect-adsorbate-mediated processes. The S/B/W layer configuration displayed here showed a slightly larger desorption signal than the S/W/B configuration. The displayed traces were averaged from those obtained from the 30 irradiation spots across the substrate to improve the signal to noise ratio. The PSD intensity is greater at 250.0 nm, consistent with the previously reported ToF data, which demonstrated enhanced H_2O desorption at this wavelength, which is on resonance with the specified C_6H_6 transition. This observed increase in desorption signal intensity for 250.0 nm is consistent with the higher photon absorption cross section at this wavelength. Desorption cross sections were obtained by fitting the experimental PSD traces with the following functional form:

$$I(t) = I_0 \exp[-\sigma\phi t] + I_\infty,$$

where $I(t)$ is the PSD signal at time t, σ is the desorption cross section, ϕ is the photon flux, and I_∞ is the signal at infinite time. The photon fluxes were determined for each wavelength from the irradiance associated with the measured pulse energy. For irradiation wavelengths of 250.0 and 248.8

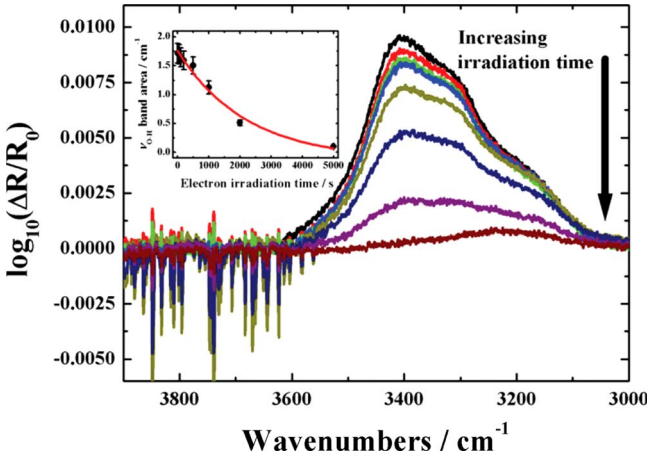

FIG. 2. (Color online) RAIR spectra showing the O–H stretching band of ASW as a function of increasing irradiation time with 250 eV electrons. The irradiation times are 0, 50, 100, 200, 500, 1000, 2000, and 5000 s. The inset shows band decay as a function of irradiation time (solid circles) along with the fitted exponential decay function (solid line). The sharp features at large wavenumber values result from fluctuations in the concentration of gas phase H_2O in the IR beam path external to the UHV chamber.

nm, the typical calculated fluxes were the same to within experimental error yielding a typical value of $(4.5 \pm 0.5) \times 10^{18}$ photons cm^{-2} s^{-1}. The H_2O desorption cross sections obtained in this way were $(1.3 \pm 0.5) \times 10^{-19}$ and $(9.6 \pm 3) \times 10^{-20}$ cm^2 for 250.0 and 248.8 nm, respectively. The smaller signal obtained at 248.8 nm, also observed in the ToF traces,[23] is attributed to the QMS essentially displaying a bias toward more rapid desorption when working close to the detection limit, as is the case here. The photon order was estimated by considering the desorption yields obtained at the two pulse energies. The increase in desorption yield with photon flux is consistent with a photon order of one, although a full set of flux dependence measurements would be required to confirm this.

B. Electron-stimulated desorption

Electron-stimulated desorption experiments were performed using both a thick film of H_2O with no C_6H_6 present and a cASW film of the same thickness with a thin (approximately 1 ML) film of C_6H_6 adsorbed on top. Electron energies in the range of 200–300 eV were used. No differences between the H_2O loss rates from these two systems were observed. This indicates that desorption occurs as a direct result of the interaction between electrons and H_2O molecules and that C_6H_6 is not involved in the H_2O desorption in this instance. The RAIRS technique employed in these experiments allows only the determination of the total loss of H_2O on the surface and so includes contributions from both desorption and reactive losses. Figure 2 shows a typical sequence of RAIR spectra, for the O–H stretch region, obtained during the irradiation of the H_2O film with 250 eV electrons. The RAIR spectra are in agreement with the previous infrared investigations of ASW films.[40] The exponential decay of this band, indicative of total H_2O loss, is shown in the inset. The decay was fitted with the function described previously to obtain the total loss cross section. The cross sections obtained were $(2.4 \pm 1) \times 10^{-18}$, $(4.7 \pm 3) \times 10^{-18}$, and $(10.2 \pm 3) \times 10^{-18}$ cm^2 for electron energies of 200, 250, and 300 eV, respectively. While further investigations at a larger number of electron energies are certainly warranted, the results presented here suggest a monotonic increase in cross section with increasing electron energy.

IV. DISCUSSION

The ESD data presented here indicate a monotonic increase in H_2O desorption cross section. It is important to recognize that an incident electron may lead to multiple ionization events within the ice, and ultimately an increased rate of desorption. More energetic electrons will therefore result in an increased ionization rate, consistent with the observed trend. However, in order to understand the obtained values for the PSD cross sections, it is necessary to consider the mechanism by which photon absorption by C_6H_6 molecules leads to H_2O desorption.

The photon-irradiation results reported here were obtained during the same experiments as our recently published studies of the dynamics of photodesorbed C_6H_6 and H_2O.[23,24] Previously, three distinct desorption mechanisms were distinguished: the direct adsorbate-mediated desorption of C_6H_6, the indirect-adsorbate-mediated desorption of H_2O, and the substrate-mediated desorption of both C_6H_6 and H_2O. The small substrate-mediated desorption component observed was consistent with the small absorption coefficient of sapphire which varies little across the wavelength range studied.[41] Adsorbate-mediated H_2O desorption was only observed when C_6H_6 was present, consistent with H_2O having a negligible photon absorption cross section at these wavelengths. The unimolecular decomposition of a surface bound $C_6H_6 \cdots (H_2O)_n$ cluster, where n is approximately 6–7, was shown to be consistent with the observed ToF profiles. Here we have focused solely on the nonthermal desorption kinetics of H_2O, in particular, the S/B/W system which produced the largest yield of H_2O.

While the photon absorption cross section alone, which is greater at 250.0 nm, determines the overall intensity of the desorption signal, the desorption cross section depends intimately on the desorption mechanism, in this case the unimolecular decomposition discussed previously. Given that photons are absorbed by C_6H_6 molecules, it is useful to consider the electronic energy levels involved, namely, S_0 and S_1 corresponding to the ground electronic state and the first excited-electronic state accessed *via* the $\pi \rightarrow \pi^*$ transition. Figure 3 shows the photophysical pathways that are possible following photon absorption at 250.0 and 248.8 nm. The excited complex may immediately undergo internal conversion (IC_1) to an excited vibrational state in S_0, or relax as a result of collision induced vibrational relaxation (CIVR) to the ground vibration state in S_1 prior to IC_2. Following IC, the complex will contain internal energy denoted by $E_{int\ 1}$ and $E_{int\ 2}$, for these two pathways respectively. If CIVR occurs prior to IC, then the internal energy content of the complex will not be dependent on the photon energy and the

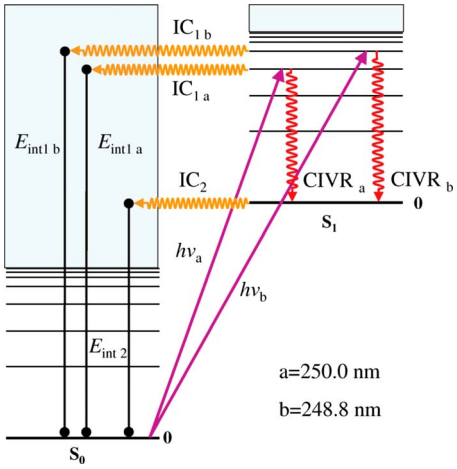

FIG. 3. (Color online) Jablonski diagram showing the possible photophysical pathways for energy redistribution within the $C_6H_6\cdots(H_2O)_n$ complex following absorption of (a) 250.0 nm and (b) 248.8 nm photons. CIVR and IC pathways are shown for both wavelengths, along with the resulting internal energy content E_{int} of the complex.

desorption cross section will be wavelength independent. However, if IC occurs before significant CIVR, as might be expected in the low temperature condensed phase, the internal energy of the complex will be greater in the case of 248.8 nm photons. A larger cross section at 248.8 nm would then be expected even though the photon absorption cross section is smaller than at 250.0 nm. Given the error estimates, it is not possible at present to determine which of these mechanisms is responsible for the observed desorption. More detailed investigations will therefore be essential in fully understanding the photophysics of the desorption process.

In order to assess the astrophysical implications of the cross sections reported in Sec. III, simple kinetic models were constructed to investigate which of the mechanisms dominate the loss of H_2O from icy mantles under different dense cloud conditions. As well as the two reported here, two further mechanisms were included in the models. The relatively long wavelength photon-stimulated process reported in the present article is most likely to play a role at the edges of dense clouds where the ISRF is not strongly attenuated. It is therefore necessary to also include the shorter wavelength photon-induced desorption of H_2O which has been shown to have a quantum yield of $\sim 10^{-3}$ for Lyman-α radiation.[15] This desorption is due to the internal UV field of dense clouds and will play a role at all A_v values. Combining the quantum yield with the corresponding photon absorption cross section for H_2O ice at this wavelength[42] results in a cross section of 4×10^{-21} cm^2. Thermal desorption was also included in the models.

The cross sections for the different H_2O desorption mechanisms were converted to first order rate coefficients by considering effective photon and electron fluxes under dense cloud and ISM conditions. The ISRF flux has been calculated and, for 250 nm photons, varies from a value of 10^8 photons cm^{-2} s^{-1} outside a cloud,[22] where $A_v=0$, to 1 photon cm^{-2} s^{-1} deeper within a cloud, where $A_v=6$. The internal UV field within a dense cloud, dominated by Lyman-α radiation, has been estimated to have constant flux of 5×10^3 photons cm^{-2} s^{-1}, independent of A_v.[20]

As far as we know, there are no direct estimates of low energy electron yields within interstellar ices. It was therefore necessary to make several approximations in order to obtain an effective electron flux for use in the models. We consider that these approximations most likely result in an underestimate of the true value. 1 MeV protons were considered as prototypical cosmic ray particles passing through the ice, the flux of which is frequently taken to be 1 proton cm^{-2} s^{-1}.[43] In order to calculate the yield of secondary electrons that results from the passage of a proton of this energy through H_2O ice, it is necessary to obtain the stopping power.[44] This was calculated with the Stopping and Range of Ions in Matter (SRIM) software package,[45] yielding a value of 19.22 keV μm^{-1}. It is also necessary to obtain the so-called *W*-value, the typical energy deposited per proton driven ionization event, in order to calculate the electron yield. The *W*-value is usually considered to be two to three times the ionization potential of the molecule being ionized,[46] which, for ASW, is 11 eV.[47] From these considerations, a secondary electron yield of 900 μm^{-1} was obtained. For a typical ice mantle thickness of 100 nm, this corresponds to an effective electron flux of 90 cm^{-2} s^{-1}. Although the secondary electron yield for 1 MeV protons peaks at around 50 eV,[48] calculations have shown that the total inelastic scattering cross section for electrons in H_2O varies by less than an order of magnitude in the range of 50–1000 eV, with ionization being the dominant scattering process.[49] The results of the present experiments at higher electron energies are therefore thought to be representative of a wide range of incident electron energies. Future experiments are planned in which electron energies below 100 eV will be utilized. However, experimental modifications are required to shield against stray magnetic fields that, at present, make the electron beam current incident at the sample unreliable at low energies.

The kinetic models were built using the Chemical Kinetics Simulator software package,[50] as previously employed in the modeling of temperature programmed desorption (TPD) measurements.[39,51] The models consist of a series of single step processes of the form $A\rightarrow B$, where the rate of conversion is given by

$$-\frac{d[A]}{dt}=[A]^n\nu_n\exp\left(-\frac{E_a}{RT}\right).$$

In this expression the concentration, [A], refers to that of the adsorbed species A, n is the kinetic order of the process, ν_n is the nth order rate coefficient, E_a is the activation energy, and T is the surface temperature. The kinetic parameters used are shown in Table I. It should be noted that the electron- and photon-stimulated processes are assumed to be temperature independent, as a result of their nonthermal nature. This means that the corresponding first order rate coefficient k_1 is simply the pre-exponential ν_1 for these processes. First order rate coefficients were calculated from the experimentally ob-

TABLE I. Kinetic parameters used in the kinetic models described in text. The values for the nonthermal mechanisms are thought to be insensitive to H_2O phase as indicated. Pre-exponential factors are quoted for a series of A_v values in the case of the ISRF induced mechanism. Thermal, ISRF induced, internal UV field, and electron induced processes are denoted by subscripts therm, ISRF, int, and e, respectively.

Mechanism	Reaction	n	ν_n (molecules$^{(1-n)}$ cm$^{2(n-1)}$ s^{-1})		E_{des} (kJ mol^{-1})
Thermal processes					
ASW desorption	$ASW \rightarrow H_2O(g)_{therm}$	0	1.5×10^{30}		46.6
Crystallization	$ASW \rightarrow I_c$	0	1.0×10^{28}		37.0
I_c desorption	$I_c \rightarrow H_2O(g)_{therm}$	0	1.5×10^{30}		47.0
ISRF induced					
ASW desorption	$ASW \rightarrow H_2O(g)_{ISRF}$	1	$A_v=0$	1.0×10^{-11}	Temperature independent
I_c desorption	$I_c \rightarrow H_2O(g)_{ISRF}$		$A_v=2$	1.0×10^{-13}	
			$A_v=4$	1.0×10^{-15}	
			$A_v=6$	1.0×10^{-19}	
Internal UV induced					
ASW desorption	$ASW \rightarrow H_2O(g)_{int}$	1	2×10^{-17}		Temperature independent
I_c desorption	$I_c \rightarrow H_2O(g)_{int}$				
Electron induced					
ASW desorption	$ASW \rightarrow H_2O(g)_e$	1	4.2×10^{-16}		Temperature independent
I_c desorption	$I_c \rightarrow H_2O(g)_e$				

tained cross sections according to the following expression:

$$k_1 = \nu_1 = \sigma\varphi.$$

The same rate coefficients were used for both I_c and ASW, although there is some evidence for an enhancement of the nonthermal desorption of H_2O from ASW compared to that for crystalline films.[52] Thermal desorption was included by using the zero-order kinetic parameters E_a and ν_0 obtained by considering those previously obtained for the desorption of ASW under astrophysical conditions.[51] These have been optimized for the recently obtained H_2O TPD experiments (not shown). The crystallization of ASW to cubic crystalline ice (I_c) as well as the thermal desorption of both ASW and I_c were also included in the model.

Simulations were initially performed at a constant temperature of 10 K to consider the nonthermal desorption mechanisms in isolation. Warm-up and the associated thermal desorption were incorporated by increasing the temperature at a typical astrophysical rate of 1 K/10^3 yr.[53] An initial ASW film H_2O concentration of 3.4×10^{17} molecules cm^{-2} was used, which represents a film thickness of the order of 10^2 layers, comparable to the typical ice mantle thickness of 100 nm found around interstellar grains. Simulations were performed with A_v values of 0, 2, 4, and 6 in order to assess the impact of the attenuation of the ISRF as a function of distance from the edge of a cloud toward its center. The model output provides the number of H_2O molecules desorbed per unit area of a grain as a function of time.

Figure 4(a) shows the fractions of H_2O desorbed by the nonthermal desorption mechanisms under constant temperature conditions. It is clear that the ISRF induced desorption channel plays an important role to depths within a cloud, where A_v exceeds a value of 2. For $A_v>4$ the internal UV field and electron induced desorption channels are dominant as a result of the attenuation of the ISRF within the cloud. Interestingly, the electron-stimulated contribution is at least an order of magnitude more efficient than that of the internal UV field at all A_v values. The fractions of H_2O desorbed by the thermal and nonthermal mechanisms as a function of A_v are shown in Fig. 4(b) under conditions where the tempera-

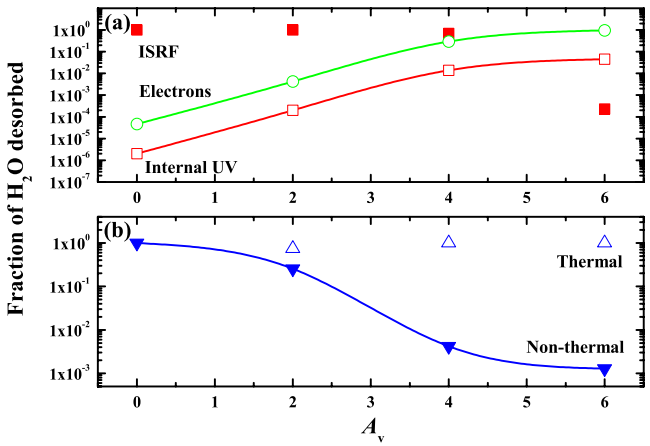

FIG. 4. (Color online) (a) Contributions of the nonthermal desorption mechanisms under constant temperature (10 K) conditions. The ISRF (closed squares), internal UV field (open squares), and electron (open circles) induced components are shown. (b) The fraction of H_2O desorbed as a result of thermal (open triangles) and nonthermal (closed triangles) desorption as a function of A_v for a heating rate of 1 K/10^3 yr. In both (a) and (b) the solid lines are provided to guide the eye. In both cases, the logarithmic scale of the ordinate should be noted.

ture was allowed to rise at a rate of 1 $K/10^3$ yr. Although thermal desorption dominates for A_v values in excess of 2, this figure shows that an understanding of nonthermal desorption mechanisms is important in gaining insight into the desorption of interstellar ices, particularly in the outer regions of dense clouds. These models confirm the importance of further investigations into the two desorption mechanisms introduced in this article; the ISRF induced desorption of H_2O resulting from an indirect-adsorbate-induced desorption process involving photon absorption by other species and the direct electron-stimulated desorption of H_2O. While C_6H_6 was used as the absorbing species in the photon-irradiation experiments reported here, the former mechanism is likely to apply for a wide range species found within interstellar ices. A more detailed discussion of the astrophysical implications will appear in a future publication.

It should be noted that the treatment of the indirect photon-induced desorption process is a gross simplification. In the ISM the ISRF varies as a function of wavelength and, as we have shown, so does the desorption cross section. Furthermore, the process will be dependent on the nature of the absorbing species and the concentration of these species within the H_2O ice. Readsorption has not been included in these models. Readsorption would result in a steady state being established at constant temperature rather than complete desorption occurring. However, the simple model presented here is useful in providing some insight into the importance of the different desorption mechanisms under astrophysically relevant conditions. Further experiments will be crucial in understanding more fully the impact of these processes in an interstellar context. We are also initiating discussion with the astronomy community to further improve our models.

V. CONCLUSIONS

Cross sections for the desorption and total loss of H_2O from an ice film as a result of two mechanisms have been measured. The first mechanism, the dynamics of which has been reported previously, is an indirect-adsorbate-mediated desorption process involving, in this case, C_6H_6. In this mechanism, photon absorption by the C_6H_6 molecule leads to H_2O desorption at wavelengths where H_2O absorption is negligible. Although the dependence of the desorption cross section on the C_6H_6:H_2O ratio has not yet been investigated, it is important to note that absorption by more complex species occurs at longer wavelengths. Indirect photodesorption is therefore likely to be an important mechanism involving other species found in interstellar ices as the ISRF is significantly more intense in the visible even to A_v values as high as 50.[22] More detailed experiments investigating the photon irradiation of more realistic ice mixtures, along with concentration dependence measurements, will be crucial in fully understanding the potential impact of this mechanism in the ISM. The second mechanism involves the direct loss of H_2O as a result of electron-stimulated desorption and reaction. Simple kinetic models, used to simulate the relevant astrophysical conditions, indicate that the ISRF induced mechanism may play an important role in the diffuse ISM, and at the edges of clouds to A_v values of between 2 and 4. The electron-stimulated component results in significant desorption at all A_v values and appears to be at least as efficient as the previously investigated desorption induced by the internal short wavelength UV field.

Dynamical experiments are anticipated in order that the translational temperatures of H_2O molecules desorbed as a result of electron impact can be determined. An understanding of the partitioning of absorbed energy between desorbing species and the substrate is crucial in an environment exhibiting such low temperatures as the ISM. Further investigations into the indirect-adsorbate-mediated desorption mechanism using larger absorbing species, for example, PAHs such as naphthalene, would allow a greater understanding of the influence of the ISRF on desorption.

ACKNOWLEDGMENTS

The authors gratefully acknowledge the STFC for its financial support in developing the UHV facilities at the CLF and for the assistance of I. P. Clark and A. W. Parker. J.D.T. and M.P.C. acknowledge the support of EPSRC-GB. D.J.B. acknowledges the support of the Leverhulme Trust. M.P.C. and F.J. acknowledge the financial assistance of the University of Nottingham. A.D. acknowledges the support of a PPARC Research Fellowship. P.J.H. and P.K. acknowledge the support of the ESF Program EIPAM. A.G.M.A. acknowledges the financial support of the Libyan Cultural Affairs Department in London.

[1] D. A. Williams and E. Herbst, Surf. Sci. **500**, 823 (2002).
[2] R. J. Gould and E. E. Salpeter, Astrophys. J. **138**, 393 (1963).
[3] V. Pirronello, O. Biham, C. Liu, L. Shen, and G. Vidali, Astrophys. J. **483**, L131 (1997).
[4] B. T. Draine, Annu. Rev. Astron. Astrophys. **41**, 241 (2003).
[5] H. J. Fraser, M. P. Collings, M. R. S. McCoustra, and D. A. Williams, Mon. Not. R. Astron. Soc. **327**, 1165 (2001).
[6] M. P. Collings, M. A. Anderson, R. Chen, J. W. Dever, S. Viti, D. A. Williams, and M. R. S. McCoustra, Mon. Not. R. Astron. Soc. **354**, 1133 (2004).
[7] W. A. Brown and A. S. Bolina, Mon. Not. R. Astron. Soc. **374**, 1006 (2007).
[8] A. J. Wolff, C. Carlstedt, and W. A. Brown, J. Phys. Chem. C **111**, 5990 (2007).
[9] K. I. Öberg, F. van Broekhuizen, H. J. Fraser, S. E. Bisschop, E. F. Van Dishoeck, and S. Schlemmer, Astrophys. J. **621**, L33 (2005).
[10] K. Willacy and D. A. Williams, Mon. Not. R. Astron. Soc. **260**, 635 (1993).
[11] C. Dominik, C. Ceccarelli, D. Hollenbach, and M. Kaufmann, Astrophys. J. **635**, L85 (2005).
[12] K. Kobayashi, J. Phys. Chem. **87**, 4317 (1983).
[13] M. S. Westley, R. A. Baragiola, R. E. Johnson, and G. A. Baratta, Nature (London) **373**, 405 (1995).
[14] M. S. Westley, R. A. Baragiola, R. E. Johnson, and G. A. Baratta, Planet. Space Sci. **43**, 1311 (1995).
[15] K. I. Öberg, H. Linnartz, R. Visser, and E. F. Van Dishoeck, Astrophys. J. **693**, 1209 (2009).
[16] P. A. Gerakines, W. A. Schutte, and P. Ehrenfreund, Astron. Astrophys. **312**, 289 (1996).
[17] A. Yabushita, D. Kanda, N. Kawanka, M. Kawasaki, and M. N. R. Ashfold, J. Chem. Phys. **125**, 133406 (2006).
[18] T. Hama, A. Yabushita, M. Yokoyama, M. Kawasaki, and S. Andersson, J. Chem. Phys. **131**, 054508 (2009).
[19] A. Yabushita, T. Hama, M. Yokoyama, M. Kawasaki, S. Andersson, R. N.

Dixon, M. N. R. Ashfold, and N. Watanabe, Astrophys. J. **699**, L80 (2009).
[20]C. J. Shen, J. M. Greenberg, W. A. Schutte, and E. F. van Dishoeck, Astron. Astrophys. **415**, 203 (2004).
[21]S. S. Prasad and S. P. Tarafdar, Astrophys. J. **267**, 603 (1983).
[22]J. S. Mathis, P. G. Mezger, and N. Panagia, Astron. Astrophys. **128**, 212 (1983).
[23]J. D. Thrower *et al.*, Astrophys. J. **673**, 1233 (2008).
[24]J. D. Thrower *et al.*, J. Vac. Sci. Technol. A **26**, 919 (2008).
[25]P. Rowntree, L. Parenteau, and L. Sanche, J. Chem. Phys. **94**, 8570 (1991).
[26]G. A. Kimmel and T. M. Orlando, Phys. Rev. Lett. **75**, 2606 (1995).
[27]G. A. Kimmel, T. M. Orlando, C. Vezina, and L. Sanche, J. Chem. Phys. **101**, 3282 (1994).
[28]T. M. Orlando and M. T. Sieger, Surf. Sci. **528**, 1 (2003).
[29]G. A. Grieves and T. M. Orlando, Surf. Sci. **593**, 180 (2005).
[30]N. G. Petrik and G. A. Kimmel, J. Chem. Phys. **123**, 054702 (2005).
[31]J. Herring-Captain, G. A. Grieves, A. Alexandrov, M. T. Sieger, H. Chen, and T. M. Orlando, Phys. Rev. B **72**, 035431 (2005).
[32]D. M. Hudgins and L. J. Allamandola, in *Proceedings of the IAU Symposium No. 231: Astrochemistry: Recent Successes and Current Challenges*, edited by D. C. Lis, G. A. Blake, and E. Herbst (Cambridge University Press, Cambridge, 2006), p. 443.
[33]E. Dwek *et al.*, Astrophys. J. **475**, 565 (1997).
[34]J. M. Greenberg and A. Li, Adv. Space Res. **24**, 497 (1999).
[35]C. J. Craven, P. D. Hatton, C. J. Howard, and G. S. Pawley, J. Chem. Phys. **98**, 8236 (1993).
[36]G. A. Kimmel, K. P. Stevenson, Z. Dohnálek, R. S. Smith, and B. D. Kay, J. Chem. Phys. **114**, 5284 (2001).
[37]N. J. Mason (unpublished).
[38]D. J. Oakes, Ph.D. thesis, University of East Anglia, 1994.
[39]J. D. Thrower, M. P. Collings, F. J. M. Rutten, and M. R. S. McCoustra, Mon. Not. R. Astron. Soc. **394**, 1510 (2009).
[40]A. S. Bolina, A. J. Wolff, and W. A. Brown, J. Phys. Chem. Br. **109**, 16836 (2005).
[41]B. S. Patel and Z. H. Zaidi, Meas. Sci. Technol. **10**, 146 (1999).
[42]N. J. Mason *et al.*, Faraday Discuss. **133**, 311 (2006).
[43]V. Mennella, G. A. Baratta, A. Esposito, G. Ferini, and Y. J. Pendleton, Astrophys. J. **587**, 727 (2003).
[44]R. E. Johnson (private communication).
[45]Stopping and Range of Ions in Matter (SRIM) 2006 software, available online at www.srim.org.
[46]W. F. Schmidt and E. Illenberger, Nukleonika **48**, 75 (2003).
[47]M. Vinodkumar, K. N. Joshipura, C. G. Limbachiya, and B. K. Antony, Nucl. Instrum. Methods Phys. Res. B **212**, 63 (2003).
[48]K. A. Long and H. G. Paretzke, J. Chem. Phys. **95**, 1049 (1991).
[49]M. Dingfelder, A. Travia, R. A. McLawhorn, J. L. Shinpaugh, and L. H. Toburen, Radiat. Phys. Chem. **77**, 1213 (2008).
[50]Chemical Kinetics Simulator (CKS), version 1.0, IBM Almaden Research Center, 650 Harry Road, Mailstop ZWX1D1, San Jose, CA. Further information may be obtained from the CKS website at http://www.almaden.ibm.com/st/msim/ckspage.html.
[51]M. P. Collings, J. W. Dever, H. J. Fraser, and M. R. S. McCoustra, Astrophys. Space Sci. **285**, 633 (2003).
[52]J. Bergeld and D. Chakarov, J. Chem. Phys. **125**, 141103 (2006).
[53]S. Viti, M. P. Collings, J. W. Dever, M. R. S. McCoustra, and D. A. Williams, Mon. Not. R. Astron. Soc. **354**, 1141 (2004).